www.czasopisma.pan.pl PAN POLSKA AKADEMIA NAUK www.journals.pan.pl

Archives of Acoustics Vol. 48, No. 4, pp. 497–507 (2023), doi: 10.24425/aoa.2023.146814

Research Paper

Investigation of the Acoustic Properties of a Metamaterial with a Multi-Ring Structure

Grzegorz SZCZEPAŃSKI*, Marlena PODLEŚNA, Leszek MORZYŃSKI, Anna WŁUDARCZYK

Central Institute For Labour Protection – National Research Institute
Warsaw, Poland

*Corresponding Author e-mail: grszc@ciop.pl

(*received December 13, 2022; accepted May 30, 2023*)

In this article, the authors present the geometry and measurements of the properties of an acoustic metamaterial with a structure composed of multiple concentric rings. CAD models of the structure were developed and subsequently used in numerical studies, which included the study of resonant frequencies using the Lanczos method and an analysis of sound pressure level distribution under plane wave excitation using the finite element method. Subsequently, experimental tests were carried out on models with the same geometry produced with three different materials (PLA, PET-G, and FLEX) using a fused deposition modeling 3D printing technique. These tests included: determining insertion loss for a single model based on tests using the measurement window of a reverberation chamber and determining transmission loss through tests in a semi-anechoic chamber. Sound wave resonance was obtained for frequencies ranging from 1700 to 6000 Hz. Notably, the experimental studies were carried out for the same structure for which numerical tests were conducted. The physical models of a metamaterial were manufactured using three different readily available 3D printing materials. The results of laboratory tests confirm that the created acoustic metamaterial consisting of multi-ring structures reduces noise in medium and high frequencies.

Keywords: acoustic metamaterials; numerical research; experimental research; finite element method; multi-ring structures.

1. Introduction

Noise is the most common hazard in the work environment, accounting for 55.1% of all identified hazards related to the work environment in Poland (GUS, 2019). One of the commonly used protections designed to reduce noise emitted by machines in industrial conditions are sound-insulating enclosures and barriers, which are referred to as passive noise protection (Engel *et al.*, 2009). The use of this type of protection is a solution, where the threat of noise is eliminated by preventing its propagation thus preventing further signal transmission. Noise transmission can also be reduced using active methods (Wrona, Pawełczyk, 2019; Morzyński, Szczepański, 2018; Mazur *et al.*, 2018).

The common practice in the case of passive methods was the use of solid materials with sound insulation or sound absorption properties. The effectiveness of a given solution depends on the thickness of the layer and the type of material used (Sikora, 2011). However, sometimes such solutions are not recommended or possible to implement, due to, e.g., costs, issues with heat dissipation or weight. Acoustic metamaterials offer a solution to such challenges, as their sound attenuation properties mainly depend on their internal structure rather than the material's type or properties (Nakayama *et al.*, 2021; Iannace *et al.*, 2021; Liu *et al.*, 2020; Szytler, Strumiłło, 2022; Zhang *et al.*, 2020). A metamaterial can take the form, for example, a flat or spatial structure made from a non-sound-absorbing material, e.g., one produced using the 3D printing technique (Zieliński *et al.*, 2020). Acoustic metamaterial is constructed to absorb sound in a specific frequency band. In the most frequently studied and developed metamaterials containing resonant

structures, these properties are observed notably in narrow frequency bands, closely aligned with the resonance frequencies of the structures used in their construction. For example, acoustic metamaterials based on Helmholtz resonators ensure high sound absorption with a small structure thickness compared to the acoustic wavelength (Duan *et al.*, 2021; Mahesh, Mini, 2019).

Another type of a metamaterial is a metamaterial with a maze structure, composed of multiple acoustic channels with twisted, meandering paths. A metamaterial can also be made of a porous material in which resonators are placed, allowing to broaden the sound absorption band in the medium and low frequency spectrums (Gao *et al.*, 2022). Structures related to acoustic metamaterials are sonic crystals. They consist of periodically arranged structures, often in the form of elongated rings arranged on a grid, dispersing acoustic waves. Similar to acoustic metamaterials, sonic crystals exhibit sound attenuation properties in a narrow frequency band. Adjusting the crystal's attenuation band is often addressed in research works (Radosz, 2019). Efforts are frequently made to manipulate the geometry of sonic crystals, for example, by changing the thickness and the material of the crystal filling (Pennec *et al.*, 2004). So far, single-ring structures used in metamaterial construction have been extensively studied and discussed in the literature. However, the results obtained up to this point indicate that such structures may exhibit sound attenuation properties across multiple frequency bands, in contrast to single-ring structures (Chen *et al.*, 2018). Studies on polycyclic-like structures indicate that such structures are capable of attenuating sounds of lower frequencies, which is difficult to achieve in the case of metamaterials (Wang *et al.*, 2012).

In the present article, a barrier model of an acoustic metamaterial consisting of a multi-ring structure is described and subsequently investigated numerically and experimentally.

2. Investigated metamaterial model

Many workstations are separated from each other by safety barriers composed of wire mesh applied to aluminum profiles. Replacing this mesh with an acoustic metamaterial featuring an appropriate structural pattern can reduce noise at adjacent workstations. The main objective in developing the metamaterial cell is to obtain a relatively large number of resonant frequencies in the frequency range of 1 to 6.3 kHz. It was assumed that there might be a noise reduction effect near the resonant frequencies. The metamaterial cell should be as small as possible and allow to obtain multi-format barriers by creating a structure based on a large number of cells. Consequently, it was established that the cell pattern should conform to a shape of a square with a side of 25 mm (considering the width of the aluminum profiles often used in the construction of workstation partitions).

The cell of such a size can be used, for example, in constructing acoustically beneficial thin workstation partitions or as a sliding industrial curtain. Since the goal of the study is to create a structure with multiple resonant frequencies, it is hypothesized that a structure with multiple chambers (particularly ring-shaped ones) could achieve this goal, and consequently a ring-based structure is proposed as the base shape for the cell. The developed structure consisted of three thin-walled concentrically placed rings connected to a small cylinder, also placed concentrically inside the smallest ring. These rings were connected to each other and to the side walls via arch-shaped walls with openings. The rings have cutouts in several places to allow for airflow. The analyzed model is composed of six structures (metamaterial cells) arranged in a sequence that is 150 mm tall and 140 mm wide, and with a thickness of 25 mm. The geometric model of the developed solid model of a single multi-ring cell and the structure consisting of several multi-ring cells in cross-section is shown in Fig. 1.

The model designed in CAD software was used as the basis for both numerical analysis and constructing three physical models. These physical metamaterial models were created using 3D printing in fusion deposition modeling (FDM) technology, using three types of materials: PLA (a biodegradable polymer), PETG (a transparent polymer with glycol addition), and FLEX (a rubber-like material with a hardness of 40D). A nozzle with a diameter of 0.4 mm was used to create the models. The only places where the use of filling was required (given that the model is thin-walled) were the cylinders located at the center of the rings filled in 100%. The models created for laboratory experiments are shown in Fig. 2.

3. Method

Three types of studies were conducted with the proposed structure: numerical analyses were carried out on the CAD model, and insertion loss and transmission loss studies were implemented using physical models. In numerical analysis, resonant frequencies were first examined, and then they were used for the analysis in frequency domain analysis to assess the distribution of the sound pressure level behind the tested model. In the numerical study, the model was positioned in such a way that the cutouts in the front of the model (Fig. 1, side A) faced the excitation source.

In the experimental studies, measurements were made for two configurations of the metamaterial model: one with the cutouts facing the excitation source and the other with the model's back (Fig. 1, side B) facing the excitation source. The study focused

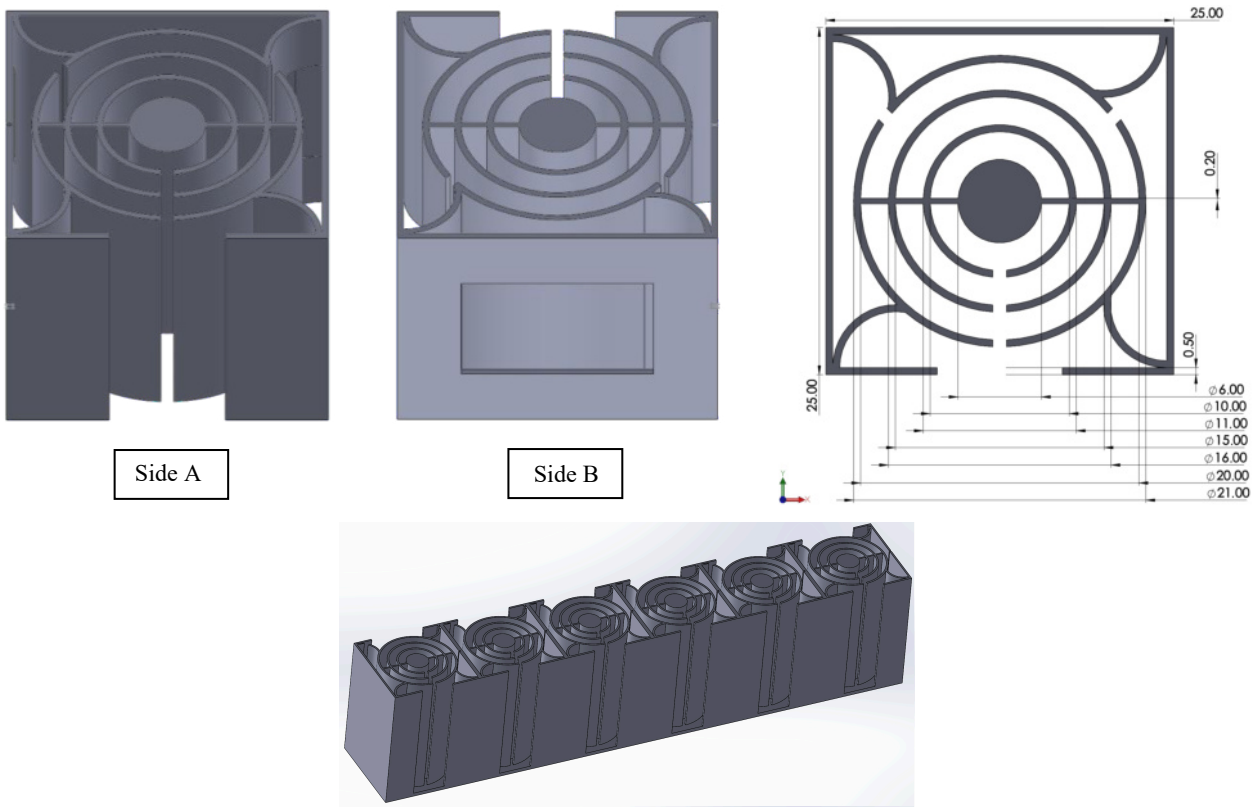

Fig. 1. View of a single metamaterial cell (top) and a structure composed of several cells (bottom).

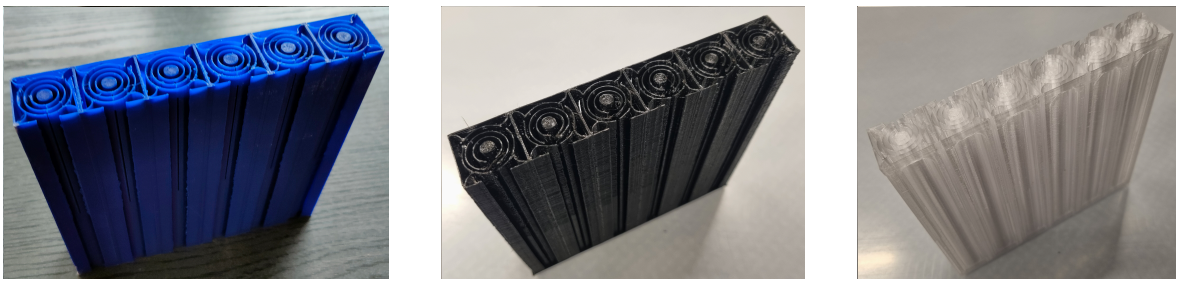

Fig. 2. Created models of an acoustic metamaterial with a multi-ring structure made out of three different materials (from the left): PLA, FLEX, and PETG.

on determining the transmission loss to check whether the properties of the material used to create the metamaterial influenced its insulating properties. Transmission loss and insertion loss were measured in different sound fields (free and diffuse) to simulate different industrial conditions. Where the replacement of the wire mesh with an acoustic metamaterial (which does not attenuate noise) is considered, the results of the insertion loss study may be. Conversely, in the case of replacing existing barriers, the results of the transmission loss study are more appropriate.

3.1. Numerical analysis

Two types of numerical analyses were performed on the developed CAD models. These studies were conducted using the Siemens Simcenter 3D environment with solvers SOL103 and SOL108. The first numerical test was aimed to determine the resonant frequencies for a single cell of an acoustic metamaterial as well as for a 6-cell structure using the Lanczos method. The second study was conducted in the frequency domain using the finite element method involving a plane wave excitation with a sound pressure of 2 Pa. The inlet, outlet and side walls of the CAD model were defined as acoustic absorbers. Restraints (permanent constraints) were established for the tunnel's extremities. The FEMAO adaptive technique was used in the calculations.

The performed numerical analyses were of the two-way coupled type (the interaction of the structure and fluid domains). Global connection parameters between the fluid domain and the solid domain were adopted using the default (recommended) coupling method. Be-

fore starting the tests, the quality of the computational mesh was checked, which showed no errors. The excitation tests were performed in the frequency domain in the range from 100 to 6500 Hz in 1/12 octave bands. The recommended criterion regarding the width of the computational grid (Howard, Cazzolato, 2017) (dimension smaller than 1/6 of the wavelength) was met in the tests.

3.2. Sound insertion loss study

The insertion loss studies for the physical model of the acoustic metamaterial barrier made from PLA were carried out using a measurement window in a reverberation chamber. The measurement window took the form of a rectangle measuring 14 cm by 15 cm and was created by two walls (14 and 26 cm thick) separated by an air gap (3 cm thick). The dimensions of the samples were adjusted to match the frame so that no additional mounting elements were needed to attach them. The model was pressed into the mounting frame attached to the outer wall of the chamber. The space between the mounting frame and the chamber wall was sealed with sealing material. The diagram of the measurement stand is shown in Fig. 3.

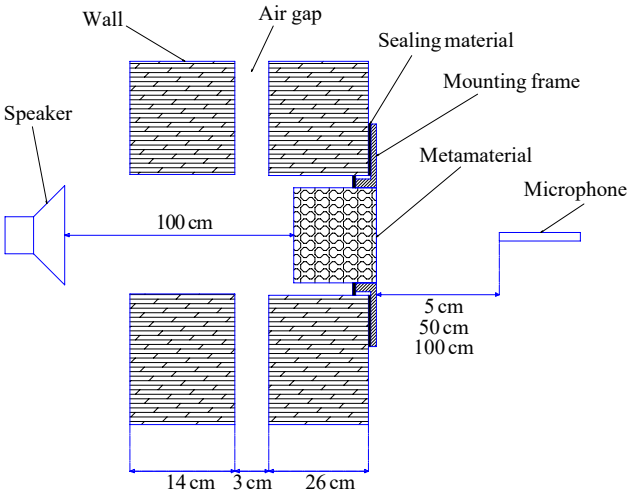

Fig. 3. Diagram of the stand for measuring the insertion loss in the measurement window of the reverberation acoustic chamber.

The reverberant acoustic chamber was treated as a transmission room and a sound source in the form of a loudspeaker was placed in it at a distance of 1 m from the first opening in the wall. The loudspeaker's membrane was facing the central part of the model. The receiving room was designated as the laboratory room. Sound pressure level measurements were conducted using the PULSE B&K system (a 3052-A-030 cassette and a 1/2 inch TEDS 4191 microphone). In order to avoid obtaining measurement results for a point that may be a local attenuation/amplification (especially close to the structure) the measurements were performed at three measurement points. The microphone was placed on the side of the receiving room at distances of 5, 50, and 100 cm from the model being measured, perpendicular to its surface, and aligned coaxially with the point of intersection of the diagonals of the model's surface. Pink noise was used as the excitation signal. The duration of the measurement was 30 s for each measurement point in the study of each model and 1 min for the background noise level measurements.

The measurements were carried out in the range from 100 to 6500 Hz. After the measurements, the insertion loss was determined as the difference in sound pressure level of the noise emitted by the loudspeaker with and without the use of a metamaterial model for each of the measurement points.

3.3. Sound transmission loss

The impulse response method (the Dirac delta function method) was used as the research method for determining the transmission loss. The measurements were carried out in a semi-anechoic chamber. A loudspeaker positioned in front of the tested model was used as the sound source. The models were mounted on an arm in the form of a pipe, aligned with the axis of symmetry of the loudspeaker membrane, 2 m from the loudspeaker, and at the same height as the loudspeaker. The measurement stand scheme is shown in Fig. 4.

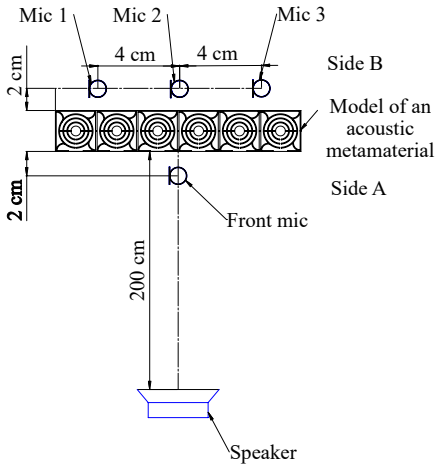

Fig. 4. Measurement stand scheme in the semi-anechoic acoustic chamber.

An e-sweep signal (an exponential sweep, where the frequency increases exponentially over time) was used as the stimulus signal. In order to minimize the impact of the microphone on the sound field distribution, a 1/8 inch TEDS 4138-A-015 microphone was used. Two measurements were conducted at the same time – in front of and behind the model (both microphones of the same type). The microphones were connected to the NEXUS Bruel & Kjaer signal conditioner, through which the signal was sent via the RME sound card to a computer with Dirac (Bruel & Kjaer) version 5 software. Due to the small size of the model, three measurement points were placed (one opposite the center of the metamaterial and the two at points 3 cm apart from the edges of the sides of the metamaterial) about 2 cm behind the model, i.e., in the acoustic near field area. Because of the unusual geometry of the model, which could result in a highly heterogeneous distribution of acoustic field parameters, especially in close proximity to the structure, the measurements were conducted at three points. The measurements of the sound pressure level in the range from 100 Hz to 6.5 kHz in 1/12 octave bands were carried out, and the examined parameter was transmission loss – defined as the difference between the sound pressure level of noise emitted by the loudspeaker at a point located 2 cm in front of the applied metamaterial model and the sound pressure level at a point located 2 cm behind the model.

4. Results

4.1. Numerical study

As part of the conducted research on resonant frequencies, the occurrence of such frequencies was found, especially in the medium and high frequency range. Table 1 presents the values of resonant frequencies determined from numerical tests for a single multi-ring cell and structure consisting of six multi-ring cells. For computing resonant frequencies the Lanczos method was used.

Table 1. Values of resonant frequencies for the multi-ring cell models.

Model	Resonant frequencies [Hz]
The single multi-ring cell	1718, 2950, 3529, 3912, 3965, 5374, 6385
The structure consisting of six multi-ring cells	1824, 2129, 2217, 2252, 2369, 2435, 2789, 2820, 2850, 2858, 2877, 2948, 3397, 3430, 3471, 3554, 3558, 3580, 3736, 3976, 4075, 4932, 4987, 5033, 5060, 5342, 5404, 5548, 5563, 5618

For a single cell, 8 different resonant frequencies were obtained, and for a structure consisting of 6 cells 30 resonant frequencies were obtained. Examples of resonant frequencies for a single cell and the structure with six cells are shown in Figs. 5 and 6.

The presented figures indicate that resonance of sound wave for particular frequencies occurs at different areas of the structure. These frequencies were then compared with the frequencies at which the most significant reduction was noticed in sound pressure levels behind the barrier in the numerical study with excitation. Exemplar visualizations for selected frequency bands (with and without the resonant frequency component) are shown in Fig. 7.

The presented visualizations show the influence of the metamaterial with a multi-ring structure on sound pressure level behind the structure in a simplified case. As part of the visualization of sound pressure level distribution for the band with a center frequency of 218 Hz, a very small effect of the structure (less than 5 dB) is observed. At the center frequency of the 1/12 octave band equal to 1830 Hz, there is an increase in the sound pressure level in front of the structure, affecting at the same time the values of the achieved

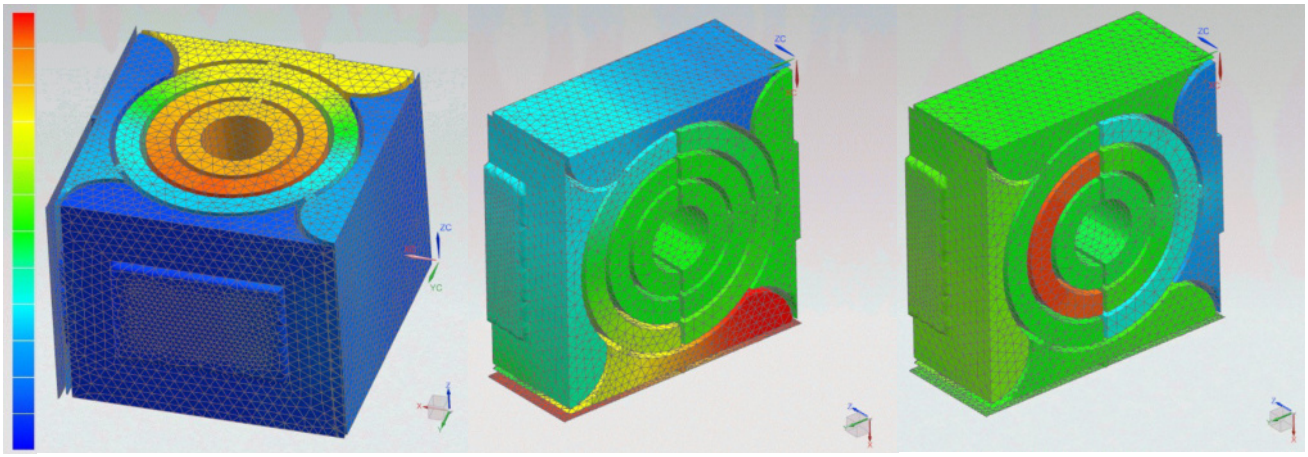

Fig. 5. Pressure distribution in the area of a single cell for the following resonant frequency (from the left): 1718, 2950, and 3529 Hz; areas of increased pressure are marked in red, and areas of ambient pressure are shown in blue.

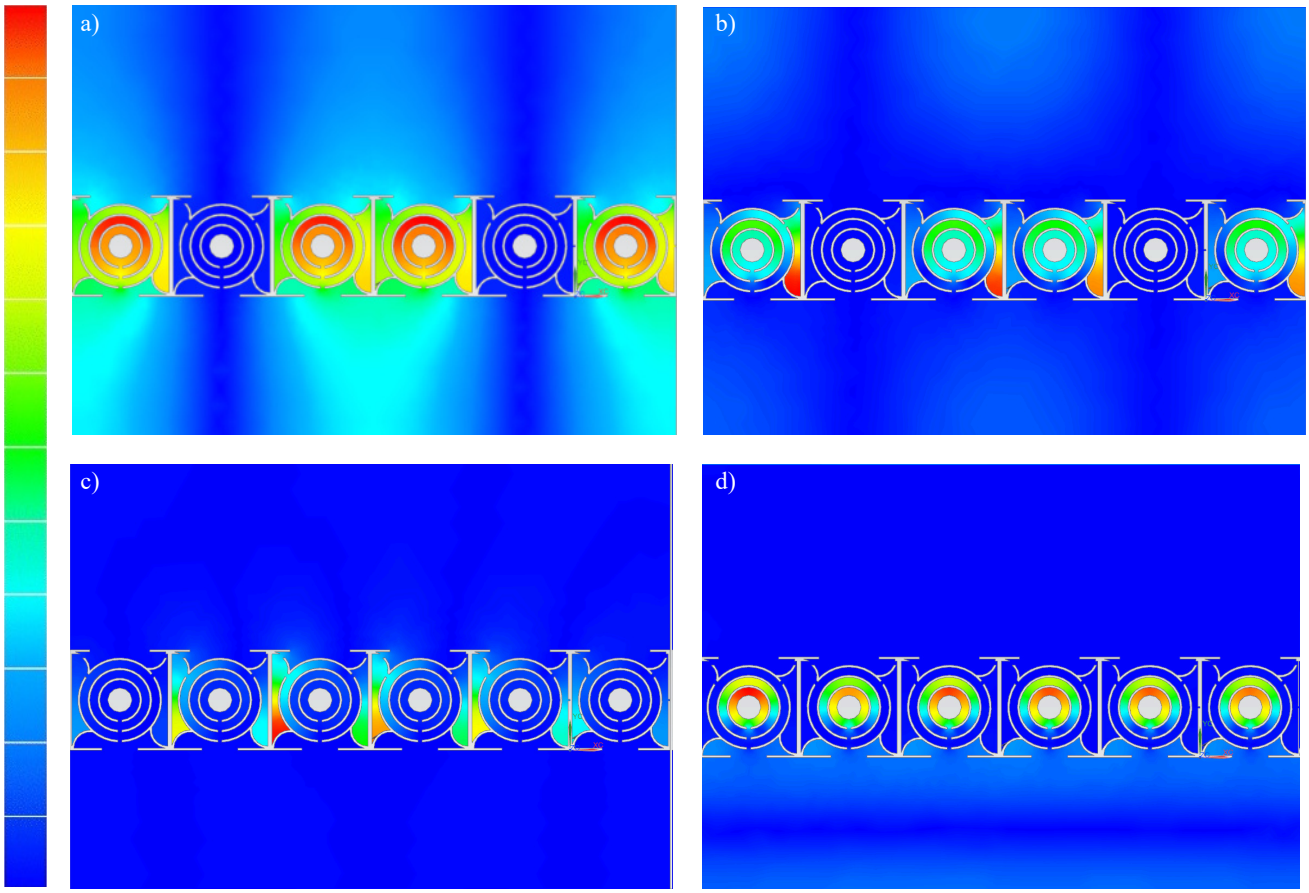

Fig. 6. Pressure distribution in the area of the six-cell structure for the following resonant frequency: a) 1824 Hz; b) 2948 Hz; c) 3580 Hz; d) 5033 Hz; areas of increased pressure are shown in red, and areas of ambient pressure in blue.

insertion loss (the insertion loss is around 10 dB). The positive influence of the structure becomes apparent at higher resonant frequencies, e.g., 3070, 3250, 3650 or 4100 Hz. The lowest values of the sound pressure level behind the acoustic metamaterial are obtained for the 1/12 octave-band's center frequency equal to 3250 Hz. The most promising results were obtained for the following center frequency bands: 3070, 3250, 3450, 3870, 4100, 4340, 4600, 4870, and 6100 Hz. It can be concluded that the presented structure most effectively impacts mid-frequency and high-frequency range.

4.2. Sound insertion loss study

The insertion loss was determined for an A-weighted sound pressure level. The research began with background noise measurements. The A-weighted sound pressure level measured was 27.3 dB. Subsequently, measurements of the noise emitted by the loudspeaker were conducted without the model for the excitation signal in the form of pink noise placed in the measurement window. The results are presented in Table 2.

The sound pressure level emitted by the loudspeaker exceeds the sound pressure level of the background noise by more than 40 dB at each measurement point. The insertion loss calculation results range from 7.5 dB (worst case) to 12.6 dB (best case). No disparity was observed between the insertion loss values for both sides of the model. The results of measurements in the form of insertion loss are presented for the 1/12 octave-band's center frequency from 103 Hz (component is below 15 dB) to 6500 Hz in Fig. 8.

Table 2. A-weighted sound pressure level for a given measurement point, without the model placed, and with the model placed on both sides.

Measurement point	A-weighted sound pressure level [dB]		
	Without the model	Side A facing the loudspeaker	Backside of the model side B facing the loudspeaker
5 cm behind the model	85.9	78.4	76.4
50 cm behind the model	74.9	64.1	64.8
100 cm behind the model	69.8	58.9	57.2

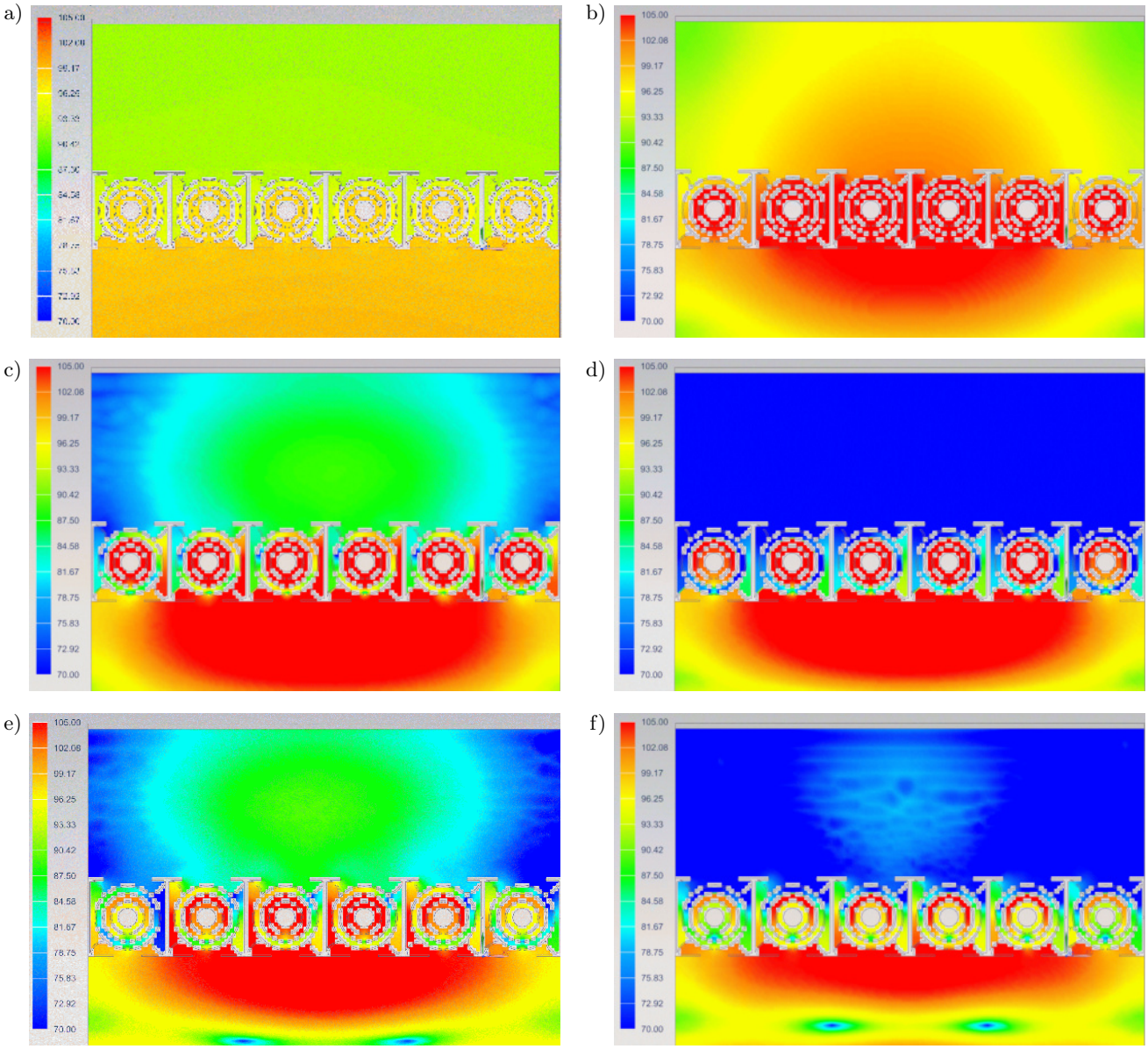

Fig. 7. Distribution of the sound pressure level obtained in a numerical test with excitation for the band with the middle 1/12 octave: a) 218 Hz; b) 1830 Hz; c) 3070 Hz; d) 3250 Hz; e) 3650 Hz; f) 4100 Hz.

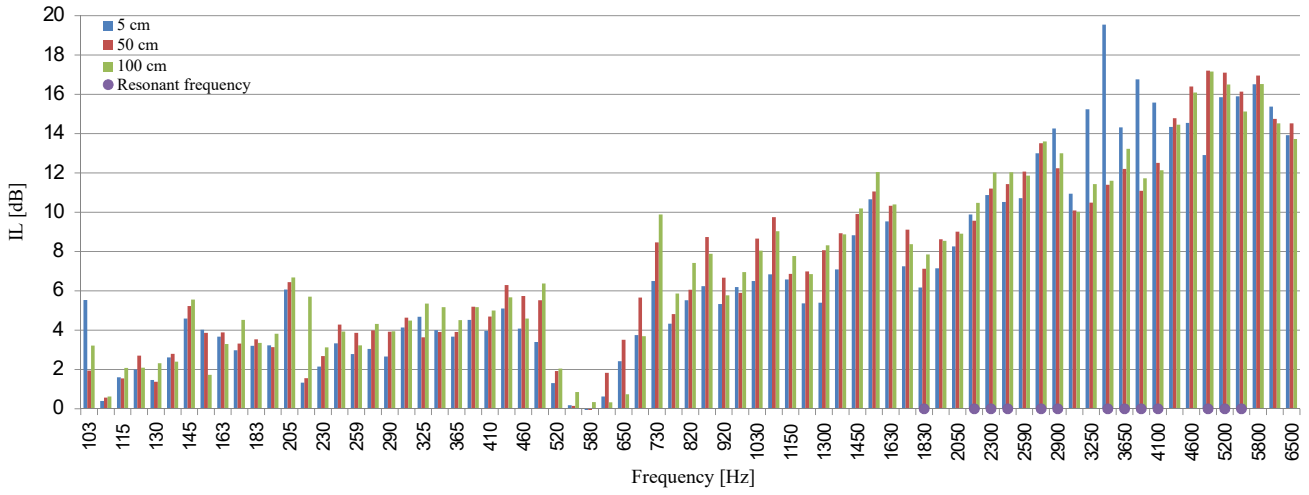

Fig. 8. Insertion loss for a distance of 100 cm behind the metamaterial with a multi-ring structure.

Figure 8 shows relatively large differences between the insertion loss values for the measurement point located 5 cm from the model and the measurement points located 50 cm and 100 cm from the model. These differences are discernable for frequency bands with center frequencies of 3250, 3450, 3650, 4100 Hz. The measurement results for the point located 5 cm away from the model indicate that the reduction takes on larger values locally, that would not be representative to properly evaluate the model. Therefore, the other two measurement points can be considered more representative for insertion loss results. In Fig. 8, the purple dots on the x-axis represent the bands in which the resonance frequencies in the numerical study were determined. Resonance frequencies in most cases occur in bands for which insertion loss was higher than 10 dB. However, the obtained results of insertion loss do not indicate a narrow-band noise reduction effect for the structure within the resonance frequencies themselves, but have a broadband character. This may be influenced by the diffusive character of the acoustic field. Notably, the highest attenuation values occur in the mid-frequency and high-frequency range.

4.3. Sound transmission loss

The measured acoustic background noise in the chamber did not exceed 20 dB. Transmission loss was determined for the A-weighted sound pressure level. Measurements behind the structure were carried out with microphones placed very close to the structure. Due to the geometry, the distribution of the acoustic field parameters behind the metamaterial structure could be very heterogeneous. Therefore, tests were performed at three measurement points. The aforementioned terminology was adopted for individual measurement points:

- Mic 1: a point located 2 cm behind the tested model on its left side (shifted by 4 cm relative to its center (the axis intersecting its center);
- Mic 2: a point located 2 cm behind the tested model, coaxially with the center of the model;
- Mic 3: a point located 2 cm behind the tested model on its right side (shifted by 4 cm relative to its center (the axis intersecting its center).

The results of the transmission loss for the $^1/_{12}$ octave-band frequencies are shown for an example measurement point (Mic 3), for models made from all three types of materials (for a single side) in Fig. 9.

The presented results show the influence of the metamaterial on the medium-frequency and high-frequency ranges. The highest transmission loss was obtained for the bands 4600, 4870, 5200, 5500, and 1830 Hz (with resonance frequencies obtained for four out of these five of bands). For bands with center frequencies of 3070, 3250, 3450, and 3650 Hz unexpected slight amplifications of the sound pressure level were observed at the Mic 3 measuring point. This is probably due to the measurements being conducted in the near-field region or it can be a constructive (amplifying) resonance effect. A similar situation was observed

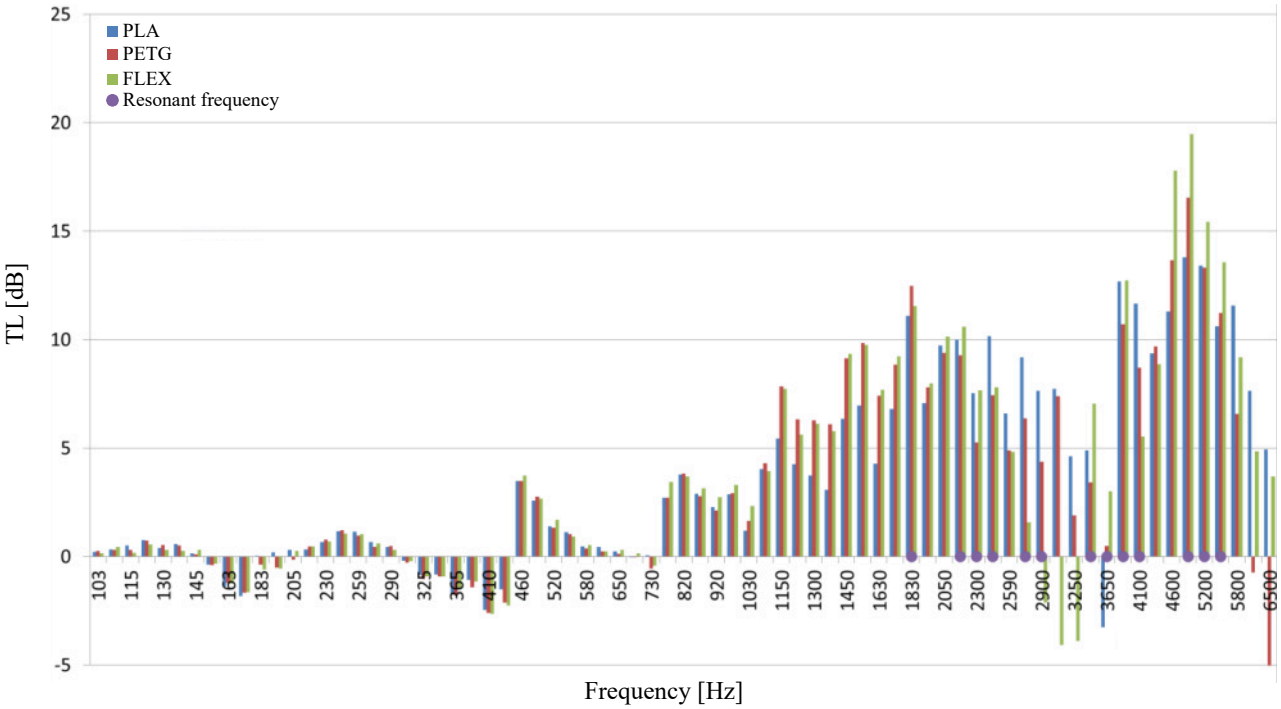

Fig. 9. Transmission loss values for models of acoustic metamaterial with a multi-ring structure made from materials (PETG, PLA and FLEX) for the Mic 3 measuring point.

for the results of measurements after the models were rotated and for the remaining measurement points. Comparison of the transmission attenuation values in 1/12 octave bands for both sides of a single model (on the example of the Mic 1 measurement point) is shown in Fig. 10.

No significant discrepancies were observed between the results obtained in the transmission loss study for side 1 (Fig. 4, side A) and side 2 (Fig. 4, side B) for each of the physical models. These differences usually did not exceed 2 dB, with the maximum difference being less than 5 dB. These variations may be attributed to the near field effect. The comparison of transmission loss obtained for an individual measurement point of a single model made from PLA on side 2 is shown in Fig. 11.

During the planning phase of the experiment, there was no assumption regarding which of the microphones would be the most representative. Each of the results is representative for a given point in the field. However, the experimental findings indicate that the results for each of the measurement points were similar. The highest values of transmission loss were obtained in the bands with center frequencies ranging from 1830 to 2440 Hz (Mic 1 – from 10.3 to 13.4 dB; Mic 2 – from 7.9 to 12.0 dB; Mic 3 – 7.9 to 11.6 dB) and 3870 to 5500 Hz (Mic 1 – 7.8 to 19.6 dB; Mic 2 – 6.7 to 10.9 dB; Mic 3 – 9.9 to 16.1 dB). For the band with the center frequency of 3650 Hz, a significant decrease in attenuation is observed for acoustic metamaterials made from each type of material (PLA, PETG, and FLEX).

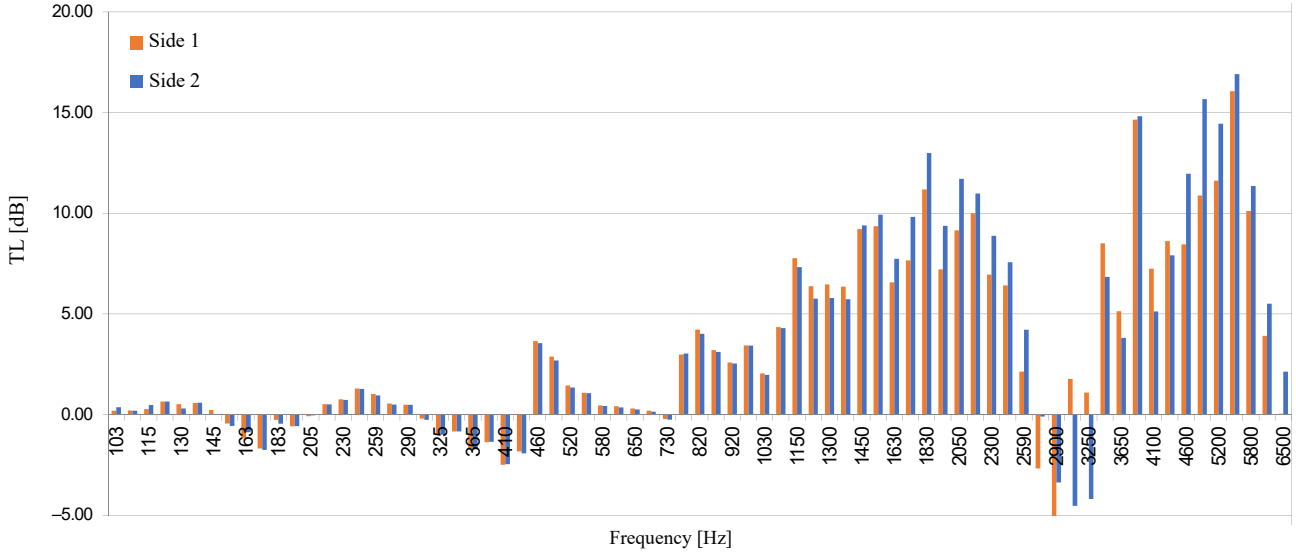

Fig. 10. Transmission loss values for a model of acoustic metamaterial with a multi-ring structure made from FLEX material at the Mic 1 measurement point for both sides of the model.

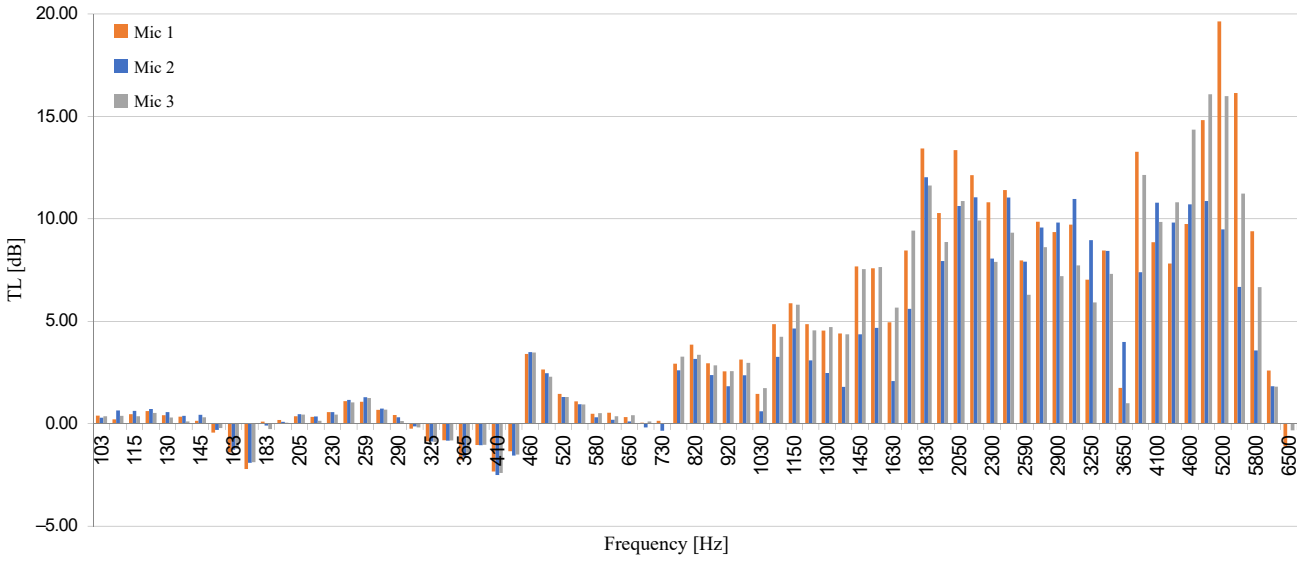

Fig. 11. Transmission loss for the acoustic metamaterial model made out of PLA determined for three measurement points.

5. Conclusions

The conducted numerical analysis with excitation can simulate the conditions similar to those in the experimental transmission loss study. However, due to the different sound pressure levels of the applied excitation and the type of the excitation signal itself (analysis using the pink noise), the values of the sound pressure level in the distributions obtained through numerical research should not be directly compared with the values obtained through experimental research. Additionally, other simplifications used in the numerical study, such as the plane wave assumption, absence of reflections, and no wave propagation on the sides of the structure cause that such results may differ significantly from the results of laboratory tests. For this reason, they were only a reference illustrating the homogeneity of the sound pressure level distribution behind the tested structure.

In most cases, the frequency band in which the highest attenuation was observed coincided with the resonant frequencies obtained through numerical research. Due to the short distance of the microphones from the tested acoustic metamaterial, the results of the transmission loss study were performed in the near field, which could have affected the obtained results. Nonetheless, their purpose was to determine the influence of the material used in the construction of the acoustic metamaterial on the attenuation results. The results prove that the material from which the acoustic metamaterial with a multi-ring structure is made from is of little importance, but the model of such a structure itself must be made with high precision. This precision requirement may pose challenges when using flexible materials in such constructions. Furthermore, the use of 3D printing technique in the production of metamaterials offers a wide range of possible modifications of such structures by affecting their resonant frequencies. The use of various types of materials commonly used in 3D printing for their production, such as rigid materials with special properties (e.g., resistant to high temperatures or weather conditions) can potentially be highly beneficial as well. The presented results for the multi-ring structure demonstrate relatively good values of insertion loss, especially in the medium-frequency and high-frequency ranges, while maintaining small gaps to allow airflow. These attributes make such structures suitable for practical application in sound-absorbing and insulating solutions.

Acknowledgments

This paper is published based on the results of a research task conducted within the scope of the 5th stage of the National Programme "Improvement of safety and working conditions", supported by resources from the National Centre for Research and Development. Task no. III.PB.05 titled "Development of acoustic metamaterial for use in soundproofing systems to control noise in industrial environments". The Central Institute for Labour Protection – National Research Institute is the main coordinator of the program.

References

1. Chen M., Meng D., Jiang H., Wang, Y. (2018), Investigation on the band gap and negative properties of concentric ring acoustic metamaterial, *Shock and Vibration*, **2018**: 369858, doi: 10.1155/2018/1369858.

2. Duan H., Shen X., Wang E., Yang F., Zhang X., Yin Q. (2021), Acoustic multi-layer Helmholtz resonance metamaterials with multiple adjustable absorption peaks, *Applied Physics Letter*, **118**(24): 241904, doi: 10.1063/5.0054562.

3. Engel Z., Piechowicz J., Pleban D., Strycznie-wicz L. (2009), *Industrial Halls, Machines and Devices – Selected Vibroacoustic Problems* [in Polish: *Hale przemysłowe, maszyny i urządzenia – wybrane problemy wibroakustyczne*], Centralny Instytut Ochrony Pracy – Państwowy Instytut Badawczy, Warszawa.

4. Gao N., Zhang Z., Deng J., Guo X., Cheng B., Hou H. (2022), Acoustic metamaterials for noise reduction: A review, *Advanced Materials Technologies*, **7**(6): 2100698, doi: 10.1002/admt.202100698.

5. GUS (Central Statistical Office) (2021), *Working Conditions in 2020*, Warsaw, https://stat.gov.pl/en/topics/labour-market/working-conditions-accidents-at-work/working-conditions-in-2020,1,15.html (access 11.10.2023).

6. Howard C.Q., Cazzolato B.S. (2017), *Acoustic Analyses Using Matlab® and Ansys®*, CRC Press.

7. Iannace G., Ciaburro G., Trematerra A. (2021), Metamaterials acoustic barrier, *Applied Acoustics*, **181**: 108172, doi: 10.1016/j.apacoust.2021.108172.

8. Liu X., Li X., Ren Z. (2020), Miniaturized spiral metamaterial array for a ventilated broadband acoustic absorber, *Shock and Vibration*, **2020**: 8887571, doi: 10.1155/2020/8887571.

9. Mahesh K., Mini R.S. (2019), Helmholtz resonator based metamaterials for sound manipulation, [in:] *Journal of Physics: Conference Series*, **1355**: 012031, doi: 10.1088/1742-6596/1355/1/012031.

10. Mazur K., Wrona S., Pawełczyk M. (2018), Design and implementation of multichannel global active structural acoustic control for a device casing, *Mechanical System and Signal Processing*, **98**: 877–889, doi: 10.1016/j.ymssp.2017.05.025.

11. Morzyński L., Szczepański G. (2018), Double panel structure for active control of noise transmission,

Archives of Acoustics, **43**(4): 689–696, doi: 10.24425/aoa.2018.125162.

12. Nakayama M. *et al.* (2021), A practically designed acoustic metamaterial sheet with two-dimensional connection of local resonators for sound insulation applications, *Journal of Applied Physics*, **129**(10): 105106, doi: 10.1063/5.0041738.

13. Pennec Y., Djafari-Rouhani B., Vasseur J.O., Khelif A., Deymier P.A. (2004), Tunable filtering and demultiplexing in phononic crystals with hollow cylinders, *Physical Review E*, **69**(4): 046608, doi: 10.1103/physreve.69.046608.

14. Radosz J. (2019), Acoustic performance of noise barrier based on sonic crystals with resonant elements, *Applied Acoustics*, **155**: 492–499, doi: 10.1016/j.apacoust.2019.06.003.

15. Sikora J. (2011), *Rubber Layers in Vibroacoustic Protection Solutions* [in Polish: *Warstwy gumowe w rozwiązaniach zabezpieczeń wibroakustycznych*], Wydawnictwa AGH, Kraków.

16. Sztyler B., Strumiłło P. (2022), Acoustic metamaterials, *Archives of Acoustics*, **47**(1): 3–14, doi: 10.24425/aoa.2022.140727.

17. Wang P., Chen T.-N., Yu K.-P., Wang X.-P. (2012), Tunable and large gaps in a two-layer semi-ring structure, *Physica Scripta*, **85**(6): 065402, doi: 10.1088/0031-8949/85/06/065402.

18. Wrona S., Pawełczyk M. (2019), Feedforward control of double-panel casing for active reduction of device noise, *Journal of Low Frequency Noise, Vibration and Active Control*, **38**(2): 787–797, doi: 10.1177/1461348418811429.

19. Zhang X., Qu Z., Wang H. (2020), Engineering acoustic metamaterials for sound absorption: From uniform to gradient structures, *iScience*, **23**(5): 101110, doi: 10.1016/j.isci.2020.101110.

20. Zieliński T.G. *et al.* (2020), Reproducibility of sound-absorbing periodic porous materials using additive manufacturing technologies: Round robin study, *Additive Manufacturing*, **36**: 101564, doi: 10.1016/j.addma.2020.101564.